SCIENCE CHINA
Physics, Mechanics & Astronomy

• Article •

April 2016 Vol. 59 No. 4: 644301
doi: 10.1007/s11433-015-00441-1

The influence of rock anisotropy on elliptical-polarization state of inhomogenously refracted P-wave

Lin Fa[1*], Jie Zhao[1], YongLan Han[1], GuoHui Li[1], PengFei Ding[1], and MeiShan Zhao[2]

[1] *School of Electronic Engineering, Xi'an University of Posts and Telecommunications, Xi'an 710121, China;*
[2] *James Franck Institute and Department of Chemistry, the University of Chicago, Chicago, IL 60637, USA*

Received October 31, 2015; accepted December 14, 2015

This paper discusses the influence of the anisotropy parameters on elliptical-polarization of the inhomogenously refracted P-wave induced at VTI-media interface. For this refracted P-wave, we have derived, the equations of the elliptical-polarization trajectory. Following the elliptical-polarization trajectory, we calculated the effects of the rock anisotropic-parameters on the polarization state, with a Poincaré-sphere-like representation, for several varying media parameters. It is noted that the size, shape and initial phase angle of the elliptical-polarization trajectory are all depending the anisotropy media, as well as on the incident-angle. We expect that the findings from this paper would be applied to practical applications of seismic exploration.

anisotropy, elliptical-polarization, inhomogenous wave, VTI medium

PACS number(s): 43.20.Bi, 43.20.Dk, 43.20Ei, 43.40.Ph

Citation: L. Fa, J. Zhao, Y. L. Han, G. H. Li, P. F. Ding, and M. S. Zhao, The influence of rock anisotropy on elliptical-polarization state of inhomogenously refracted P-wave, Sci. China-Phys. Mech. Astron. **59**, 644301 (2016), doi: 10.1007/s11433-015-00441-1

1 Introduction

In general, the polarization property of acoustic wave is similar to that of optical and/or electromagnetic waves. An acoustic wave [1-8] bears many similarities to other popular waves, such as optical wave [9], electromagnetic wave [10], thermal wave [11], capillary wave [12], and charge-density wave [13]. Nevertheless, they also posses intrinsically subtle differences. For example, optical or electromagnetic wave can propagate either in a vacuum or in a medium, whereas acoustic wave can propagate only in a medium; the optical/electromagnetic wave can only be a shear (or quasi-shear) wave, while the acoustic wave can be either shear (or quasi-shear) or longitudinal (or quasi-longitudinal).

A significant application of the acoustic wave properties is the wave propagation inside the Earth's crust. Studies of the effects of rock anisotropy on acoustic wave propagation, reflection, refraction, and polarization are critically important for proper forward modelings of both seismology and acoustic-logging, as well as interpretations of seismic exploration and logging data. Up to this point, the reported studies and discussions on the polarization of the acoustic wave have largely been limited to a homogenous wave [14-20]. Fa et al. [21] reported the effects of the rock anisotropy on the polarization of elastic homogenous P-wave and SV-wave. An anomalous incident-angle corresponding to an inhomogenously refracted P-wave was also reported [22,23].

In this paper, we discuss the effects of the rock anisotropy on the polarization states of an inhomogenously refracted P-wave induced at the interface between anisotropic-rocks. In the next Section, we review the theoretical background. Sect. 3 provides the results of calculations. Discussion and concluding remarks are given in sect. 4.

*Correspondence author (email: faxiaoxue@126.com)

2 Theory

2.1 Model for VTI-media interface

The rock as a propagation medium for acoustic wave with low frequency is generally considered as transversely isotropic. For a transversely isotropic medium with a vertical axis of symmetry which is usually abbreviated as VTI medium, a hexagonal solid state structure may be employed to describe its property [18,19,24]. Conventionally, such a system is usually modeled by an elastic stiffness tensor [25]

$$C^{(n)}=\begin{bmatrix} C_{11}^{(n)} & C_{12}^{(n)} & C_{13}^{(n)} & 0 & 0 & 0 \\ C_{12}^{(n)} & C_{11}^{(n)} & C_{13}^{(n)} & 0 & 0 & 0 \\ C_{13}^{(n)} & C_{13}^{(n)} & C_{33}^{(n)} & 0 & 0 & 0 \\ 0 & 0 & 0 & C_{44}^{(n)} & 0 & 0 \\ 0 & 0 & 0 & 0 & C_{44}^{(n)} & 0 \\ 0 & 0 & 0 & 0 & 0 & C_{66}^{(n)} \end{bmatrix}. \tag{1}$$

In eq. (1), $C_{11}^{(n)}=C_{12}^{(n)}+2C_{66}^{(n)}$ and the superscript $n=\{1, 2\}$ is used to denote the incidence and refraction media, respectively.

For the case that a harmonic P-wave propagates in *x*-*z* plane and impinges on an interface between two VTI media (see Figure 1), the particle displacements of the incidence P-wave and the four induced waves can be written as:

$$\vec{W}^{(0)}=|R^{(0)}|\begin{pmatrix} u_x^{(0)} \\ -u_z^{(0)} \end{pmatrix}\exp[\mathrm{i}(\omega t-k^{(0)}x\sin\theta^{(0)}+k^{(0)}z\cos\theta^{(0)})], \tag{2}$$

$$\vec{W}^{(1)}=|R^{(1)}|\begin{pmatrix} u_x^{(1)} \\ u_z^{(1)} \end{pmatrix} \times\exp[\mathrm{i}(\omega t-k^{(1)}x\sin\theta^{(1)}-k^{(1)}z\cos\theta^{(1)}+\phi^{(1)})], \tag{3}$$

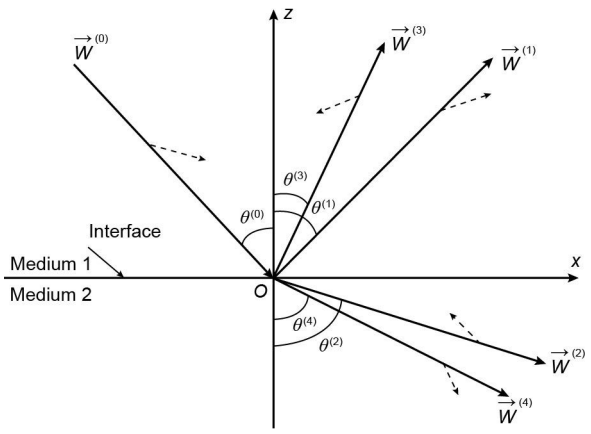

Figure 1 Polarization vector and wave-front normal for incident P-wave and four induced waves at the interface between two VTI media. The solid-lines with arrowhead indicate the phase velocity direction and the dashed-lines with arrowhead show the polarization direction.

$$\vec{W}^{(2)}=|R^{(2)}|\begin{pmatrix} u_x^{(2)} \\ -u_z^{(2)} \end{pmatrix} \times\exp[\mathrm{i}(\omega t-k^{(2)}x\sin\theta^{(2)}+k^{(2)}z\cos\theta^{(2)}+\phi^{(2)})], \tag{4}$$

$$\vec{W}^{(3)}=|R^{(3)}|\begin{pmatrix} -u_z^{(3)} \\ -u_x^{(3)} \end{pmatrix} \times\exp[\mathrm{i}(\omega t-k^{(3)}x\sin\theta^{(3)}-k^{(3)}z\cos\theta^{(3)}+\phi^{(3)})], \tag{5}$$

$$\vec{W}^{(4)}=|R^{(4)}|\begin{pmatrix} -u_z^{(4)} \\ u_x^{(4)} \end{pmatrix} \times\exp[\mathrm{i}(\omega t-k^{(4)}x\sin\theta^{(4)}+k^{(4)}z\cos\theta^{(4)}+\phi^{(4)})]. \tag{6}$$

In eqs. (2)-(6), the superscript $m=\{0, 1, 2, 3, 4\}$ denotes, respectively, the incident P-wave, reflected P-wave, refracted P-wave, reflected SV-wave and refracted SV-wave. $\theta^{(0)}$ is the incident-angle. $\theta^{(m\neq 0)}$ is a reflection/refraction angle. $u_x^{(m)}$ and $u_z^{(m)}$ are polarization coefficients. $R^{(0)}=1$ is the coefficient of incident wave and $R^{(m\neq 0)}$ is a reflection/refraction coefficient, whereas $R^{(m)}=|R^{(m)}|\exp[\mathrm{i}\phi^{(m)}]$.

For the incident P-wave and these four induced waves propagating in *x*-*z* plane without external force, Christoffel equation can be simplified as:

$$\begin{bmatrix} \Gamma_{11}^{(m)}-[v_{1,2}^{(m)}]^2 & \Gamma_{13}^{(m)} \\ \Gamma_{31}^{(m)} & \Gamma_{33}^{(m)}-[v_{1,2}^{(m)}]^2 \end{bmatrix}\begin{bmatrix} u_x^{(m)} \\ u_z^{(m)} \end{bmatrix}=0, \tag{7}$$

which leads to

$$\frac{u_z^{(m)}}{u_x^{(m)}}=-\frac{\Gamma_{11}^{(m)}-(v_{1,2}^{(m)})^2}{\Gamma_{13}^{(m)}}, \tag{8a}$$

$$\frac{u_x^{(m)}}{u_z^{(m)}}=-\frac{\Gamma_{33}^{(m)}-(v_{1,2}^{(m)})^2}{\Gamma_{13}^{(m)}}. \tag{8b}$$

The various factors in eq. (8) are defined by

$$\Gamma_{11}^{(m)}=A_{11}^{(n)}\sin^2\theta^{(m)}+A_{44}^{(n)}\cos^2\theta^{(m)}, \tag{9a}$$

$$\Gamma_{13}^{(m)}=[A_{13}^{(n)}+A_{44}^{(n)}]\sin\theta^{(m)}\cos\theta^{(m)}, \tag{9b}$$

$$\Gamma_{33}^{(m)}=A_{33}^{(n)}\cos^2\theta^{(m)}+A_{44}^{(n)}\sin^2\theta^{(m)}, \tag{9c}$$

$$\Gamma_{13}^{(m)}=\Gamma_{31}^{(m)}, \tag{9d}$$

$$A_{jl}^{(n)}=C_{jl}^{(n)}/\rho^{(n)}. \tag{9e}$$

The subscripts $\{j,l\}=\{1, 2, 3, 4, 5, 6\}$. $\rho^{(n)}$ is the density of the incidence/refraction media. $v_{1,2}^{(m)}$ is the phase velocity of the incident P-wave or each induced wave, which is described by ref. [22]

$$v_{1,2}^{(m)}=\sqrt{\frac{\Gamma_{11}^{(m)}+\Gamma_{33}^{(m)}\pm Q^{(m)}}{2}}, \tag{10}$$

$$Q^{(m)}=\sqrt{A_3^{(n)}+2A_1^{(n)}\sin^2\theta^{(m)}+A_2^{(n)}\sin^4\theta^{(m)}}. \tag{11}$$

Invoking the normalization condition

$$u_x^{(m)}[u_x^{(m)}]^* + u_z^{(m)}[u_z^{(m)}]^* = 1$$

with respect to eqs. (8) and (9), it leads to

$$(u_x^{(m)})^* u_z^{(m)} = -\frac{\Gamma_{13}^{(m)}(\Gamma_{13}^{(m)})^*}{(\Gamma_{13}^{(m)})^*[\Gamma_{33}^{(m)} - (v_{1,2}^{(m)})^2] + \Gamma_{13}^{(m)}[\Gamma_{11}^{(m)} - (v_{1,2}^{(m)})^2]^*}, \tag{12}$$

$$u_x^{(m)}(u_z^{(m)})^* = -\frac{\Gamma_{13}^{(m)}(\Gamma_{13}^{(m)})^*}{\Gamma_{13}^{(m)}[\Gamma_{33}^{(m)} - (v_{1,2}^{(m)})^2]^* + (\Gamma_{13}^{(m)})^*[\Gamma_{11}^{(m)} - (v_{1,2}^{(m)})^2]}. \tag{13}$$

The superscript '$*$' indicates a complex conjugate.

The modulus of the polarization coefficients can be given by

$$\begin{aligned} u_x^{(m)}(u_x^{(m)})^* &= [u_x^{(m)}(u_z^{(m)})^*]\frac{(u_x^{(m)})^*}{(u_z^{(m)})^*} \\ &= \frac{\Gamma_{13}^{(m)}[\Gamma_{33}^{(m)} - (v_{1,2}^{(m)})^2]^*}{(\Gamma_{13}^{(m)})^*[\Gamma_{33}^{(m)} - (v_{1,2}^{(m)})^2] + \Gamma_{13}^{(m)}[\Gamma_{11}^{(m)} - (v_{1,2}^{(m)})^2]^*}, \end{aligned} \tag{14}$$

$$\begin{aligned} u_z^{(m)}(u_z^{(m)})^* &= [(u_x^{(m)})^* u_z^{(m)}]\frac{(u_z^{(m)})^*}{(u_x^{(m)})^*} \\ &= \frac{\Gamma_{13}^{(m)}[\Gamma_{11}^{(m)} - (v_{1,2}^{(m)})^2]^*}{(\Gamma_{13}^{(m)})^*[\Gamma_{33}^{(m)} - (v_{1,2}^{(m)})^2] + \Gamma_{13}^{(m)}[\Gamma_{11}^{(m)} - (v_{1,2}^{(m)})^2]^*}. \end{aligned} \tag{15}$$

2.2 The elliptical-polarization trajectory for inhomogenously refracted P-wave

Let's discuss in detail the inhomogenously refracted P-wave, which in general is an elliptical-polarization wave. For simplification of the discussion, let's consider two distinctive incident-angle regions. We denote $\theta_c^{(2)}$ as the critical incident-angle and $\theta_a^{(2)}$ as the anomalous incident-angle. We use $a_1^{(2)}$ and $a_2^{(2)}$ to express the attenuation coefficients of the inhomogenously refracted P-wave .

2.2.1 *Right rotational elliptical-polarization*

In the incident-angle region $\theta^{(0)} \in (\theta_c^{(2)}, 90^\circ)$ for a case without an anomalous incident-angle, and in the region $\theta^{(0)} \in (\theta_c^{(2)}, \theta_a^{(2)})$ for a case where $\theta_a^{(2)}$ exists, the particle displacement components of the inhomogenously refracted P-wave is given by refs. [22,23]

$$W_x^{(2)} = |R^{(2)}| u_{xm}^{(2)} \exp[-a_1^{(2)} z]\exp[\mathrm{i}(\omega t - k^{(0)} x \sin\theta^{(0)} + \phi^{(2)})], \tag{16}$$

$$W_z^{(2)} = -|R^{(2)}| u_{zm}^{(2)} \exp[-a_1^{(2)} z] \times \exp\left[\mathrm{i}\left(\omega t - k^{(0)} x \sin\theta^{(0)} + \phi^{(2)} + \frac{\pi}{2}\right)\right]. \tag{17}$$

Taking the real parts of eqs. (16) and (17), we have

$$W_x^{(2)} = |R^{(2)}| u_{xm}^{(2)} \exp[-a_1^{(2)} z]\cos(\omega t - k^{(0)} x \sin\theta^{(0)} + \phi^{(2)}), \tag{18}$$

$$W_z^{(2)} = |R^{(2)}| u_{zm}^{(2)} \exp[-a_1^{(2)} z]\sin(\omega t - k^{(0)} x \sin\theta^{(0)} + \phi^{(2)}). \tag{19}$$

Equivalently, they can be rewritten as:

$$\left(\frac{W_x^{(2)}}{|R^{(2)}| u_{xm}^{(2)} \exp[-a_1^{(2)} z]}\right)^2 = \cos^2(\omega t - k^{(0)} x \sin\theta^{(0)} + \phi^{(2)}), \tag{20}$$

$$\left(\frac{W_z^{(2)}}{|R^{(2)}| u_{zm}^{(2)} \exp[-a_1^{(2)} z]}\right)^2 = \sin^2(\omega t - k^{(0)} x \sin\theta^{(0)} + \phi^{(2)}). \tag{21}$$

Combination of eqs. (20) and (21) leads to an elliptical equation

$$\left(\frac{W_x^{(2)}}{u_{xm}^{(2)}}\right)^2 + \left(\frac{W_z^{(2)}}{u_{zm}^{(2)}}\right)^2 = \{|R^{(2)}| \exp[-a_1^{(2)} z]\}^2, \tag{22}$$

with

$$(u_{xm}^{(2)})^2 = \frac{|\Gamma_{13}^{(2)}[\Gamma_{33}^{(2)} - (v_1^{(2)})^2]|}{|(\Gamma_{13}^{(2)})^*[\Gamma_{33}^{(2)} - (v_1^{(2)})^2] + \Gamma_{13}^{(2)}[\Gamma_{11}^{(2)} - (v_1^{(2)})^2]|}, \tag{23}$$

$$(u_{zm}^{(2)})^2 = \frac{|\Gamma_{13}^{(2)}[\Gamma_{11}^{(2)} - (v_1^{(2)})^2]|}{|(\Gamma_{13}^{(2)})^*[\Gamma_{33}^{(2)} - (v_1^{(2)})^2] + \Gamma_{13}^{(2)}[\Gamma_{11}^{(2)} - (v_1^{(2)})^2]|}. \tag{24}$$

From eqs. (18) and (19) we can obtain the angle between the elliptical trajectory extremity and x-axis:

$$\begin{aligned} \varphi &= \mathrm{atan}\left(\frac{W_z^{(2)}}{W_x^{(2)}}\right) \\ &= \mathrm{atan}\left[\sqrt{\frac{|\Gamma_{13}^{(2)}[\Gamma_{11}^{(2)} - (v_1^{(2)})^2]|}{|\Gamma_{13}^{(2)}[\Gamma_{33}^{(2)} - (v_1^{(2)})^2]|}}\tan(\omega t - k^{(0)} x \sin\theta^{(0)} + \phi^{(2)})\right]. \end{aligned} \tag{25}$$

Eqs. (22) and (25) show that the inhomogenously refracted P-wave is a right-rotational elliptical-polarized wave, i.e. it rotates in counter clockwise direction with an elliptical trajectory.

2.2.2 *Left rotational elliptical-polarization*

In the after anomalous incident-angle region for a case where $\theta_a^{(2)}$ exists, the particle displacement components of the inhomogenously refracted P-wave are given by refs. [22,23]

$$W_x^{(2)} = |R^{(2)}| u_{xm}^{(2)} \exp[-a_2^{(2)} z] \times \exp\left[\mathrm{i}\left(\omega t - k^{(0)} x \sin\theta^{(0)} + \phi^{(2)} + \frac{\pi}{2}\right)\right], \tag{26}$$

$$W_z^{(2)} = -|R^{(2)}| u_{zm}^{(2)} \exp[-a_2^{(2)} z]\exp[\mathrm{i}(\omega t - k^{(0)} x \sin\theta + \phi^{(2)})]. \tag{27}$$

The instantaneous expressions of eqs. (26) and (27) are

$$W_x^{(2)} = -|R^{(2)}| u_{xm}^{(2)} \exp[-a_2^{(2)} z]\sin(\omega t - k^{(0)} x \sin\theta^{(0)} + \phi^{(2)}), \tag{28}$$

$$W_z^{(2)} = -|R^{(2)}| u_{zm}^{(2)} \exp[-a_2^{(2)} z]\cos(\omega t - k^{(0)} x \sin\theta^{(2)} + \phi^{(2)}). \tag{29}$$

Similar to eq. (22), this leads to an elliptical-polarization trajectory and the angle between the elliptical-polarization extremity and x-axis as shown as:

$$\left(\frac{W_x^{(2)}}{u_{xm}^{(2)}}\right)^2+\left(\frac{W_z^{(2)}}{u_{zm}^{(2)}}\right)^2=\{|R^{(2)}|\exp[-a_2^{(2)}z]\}^2 \tag{30}$$

and

$$\varphi=\operatorname{atan}\left\{\sqrt{\frac{|\Gamma_{13}^{(2)}[\Gamma_{11}^{(2)}-(v_2^{(2)})^2]|}{|\Gamma_{13}^{(2)}[\Gamma_{33}^{(2)}-(v_2^{(2)})^2]|}}\cot(\omega t-k^{(0)}x\sin\theta^{(0)}+\phi^{(2)})\right\}$$
$$=\operatorname{atan}\left\{\sqrt{\frac{|\Gamma_{13}^{(2)}[\Gamma_{11}^{(2)}-(v_2^{(2)})^2]|}{|\Gamma_{13}^{(2)}[\Gamma_{33}^{(2)}-(v_2^{(2)})^2]|}}\tan\left[\frac{\pi}{2}-(\omega t-k^{(0)}x\sin\theta^{(0)}+\phi^{(2)})\right]\right\}. \tag{31}$$

Again, in eq. (30) we have

$$(u_{xm}^{(2)})^2=\frac{|\Gamma_{13}^{(2)}(\Gamma_{33}^{(2)}-(v_2^{(2)})^2)|}{|(\Gamma_{13}^{(2)})^*(\Gamma_{33}^{(2)}-(v_2^{(2)})^2)+\Gamma_{13}^{(2)}(\Gamma_{11}^{(2)}-(v_2^{(2)})^2)|}, \tag{32}$$

$$(u_{zm}^{(2)})^2=\frac{|\Gamma_{13}^{(2)}(\Gamma_{11}^{(2)}-(v_2^{(2)})^2)|}{|(\Gamma_{13}^{(2)})^*(\Gamma_{33}^{(2)}-(v_2^{(2)})^2)+\Gamma_{13}^{(2)}(\Gamma_{11}^{(2)}-(v_2^{(2)})^2)|}. \tag{33}$$

It is clear that the inhomogenously refracted P-wave is a left-rotation elliptical-polarization wave, i.e. its elliptical-polarization trajectory rotates in the clockwise direction.

3 Calculation and discussion

We have performed calculations of the polarization states, for two systems of VTI-media interface, based on the well-known anisotropic parameters reported by Thomsen [26], Vernik & Nur [27] and Wang [28], given in Tables 1 and 2. $\varepsilon^{(n)}$, $\delta^{*(n)}$ and $\gamma^{(n)}$ are the anisotropic parameters and the superscription '*' of the anisotropic parameter $\delta^{*(n)}$ does not indicate the complex conjugate of the anisotropic parameter $\delta^{(n)}$and is used for consistency with prior work [26].

The anisotropic parameters are related to the elastic moduli (see eq. (1)) by refs. [26,28]

$$C_{13}^{(n)}=\rho^{(n)}\times\sqrt{[\delta^{*(n)}(\alpha^{(n)})^4+[(\alpha^{(n)})^2-(\beta^{(n)})^2][(\varepsilon^{(n)}+1)(\alpha^{(n)})^2-(\beta^{(n)})^2]}-\rho^{(n)}(\beta^{(n)})^2, \tag{34a}$$

$$C_{33}^{(n)}=\rho^{(n)}(\alpha^{(n)})^2, \tag{34b}$$

$$C_{11}^{(n)}=[2\varepsilon^{(n)}+1]\rho^{(n)}[\alpha^{(n)}]^2, \tag{34c}$$

$$C_{44}^{(n)}=\rho^{(n)}(\beta^{(n)})^2, \tag{34d}$$

$$C_{66}^{(n)}=[2\gamma^{(n)}+1]\rho^{(n)}(\beta^{(n)})^2, \tag{34e}$$

where $\alpha^{(n)}$ and $\beta^{(n)}$ are the vertical phase velocities of P-wave and SV-wave.

For the discussion purpose in the following sections, we refer Model 1 as the case where there is no anomalous incident-angle $\theta_a^{(2)}$ or the scattering in the region between the critical incident-angle and the anomalous incident-angle. Model 2 is the case with the scattering after the anomalous incident-angle. Specifically, for the studies related to the interfaces as given in Tables 1 and 2, Table 1 has a critical incident-angle $\theta_c^{(2)}=48.34^\circ$ without an anomalous incident-angle, while Table 2 provides a case of interface with a critical incident-angle $\theta_c^{(2)}=32.10^\circ$ and an anomalous incident-angle $\theta_a^{(2)}=62.16^\circ$ [23].

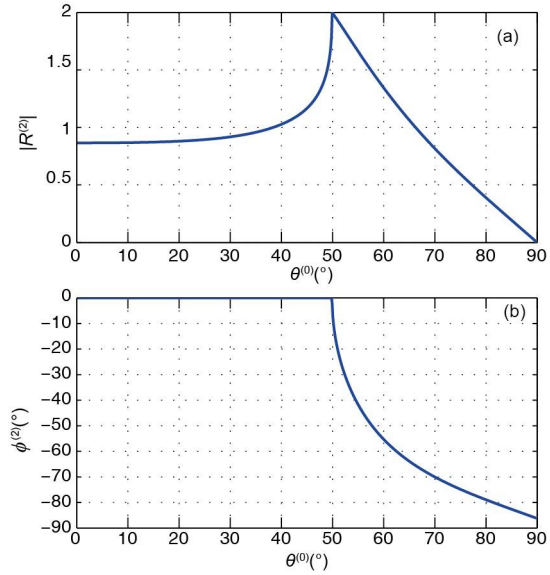

Figure 2 (Color online) Relationship of $R^{(2)}$ versus $\theta^{(0)}$ for interface between A-shale and T-sandstone. (a) Modulus; (b) phase angle.

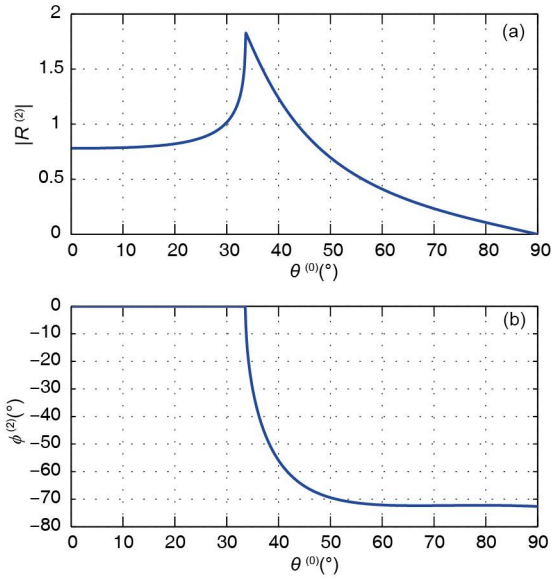

Figure 3 (Color online) Relationship of $R^{(2)}$ versus$\theta^{(0)}$ for interface between A-shale and O-shale. (a) Modulus; (b) phase angle.

3.1 Refraction coefficients of the refracted P-wave

Before detailed discussion on the influence of anisotropic media parameters with respect to the polarization state, it is always important to know the magnitude and phase angle of the refraction coefficients. Applying the algorithm as reported in ref. [20], the P-wave to P-wave refraction coefficient $R^{(2)}$ versus incident-angle $\theta^{(0)}$ for the two interfaces described by Tables 1 and 2 are calculated and presented in Figures 2 and 3.

The calculated results show that in the area of $\theta^{(0)} \in (\theta_c^{(2)}, 90^\circ)$ for these two VTI-media interfaces, the modulus of $R^{(2)}$ decreases with increasing $\theta^{(0)}$ and the value of its phase angle $\phi^{(2)}$ increases with respect to the incident-angle.

3.2 Effect of anisotropy on elliptical-polarization state

For an inhomogenously refracted P-wave, to analyze the anisotropic effect on the elliptical-polarization states, we have performed calculations for each individual anisotropy parameter, i.e. using each of the anisotropy parameters $\varepsilon^{(1)}$, $\delta^{*(1)}$, $\varepsilon^{(2)}$ and $\delta^{*(2)}$ as a variable, whereas keep other three parameters constant. Each of the anisotropy parameters is varied near the physically measured values as given in Tables 1 and 2. The calculated polarization trajectories are shown in Figures 4-6. In these figures, the two-dimension maps at the top show the rotational direction of the elliptical-polarization trajectory.

The calculated results show that the anisotropy of the incidence and refraction medium would influence not only the size of the trajectory and initial phase of the elliptical-polarization but also the shape of the trajectory.

For the interface between A-shale and T-sandstone and at the incident-angle of $\theta^{(0)} = 55.05^\circ$ (Model 1), the effects of $\varepsilon^{(1)}$ and $\varepsilon^{(2)}$ on the size, shape and initial phase angle of the

Table 1 Anisotropic parameters for interface between an anisotropic shale (A-shale) and Taylor sandstone (T-sandstone)

Medium	$a^{(n)}$ (m/s)	$b^{(n)}$ (m/s)	$r^{(n)}$ (g/cm^3)	$e^{(n)}$	$d^{*(n)}$	$g^{(n)}$
A-shale	2745	1508	2.340	0.103	- 0.073	0.345
T-sandstone	3368	1829	2.500	0.110	- 0.127	0.255

Table 2 Anisotropic parameters for interface between an anisotropic shale (A-shale) and oil-shale (O-shale)

Medium	$a^{(n)}$ (m/s)	$b^{(n)}$ (m/s)	$r^{(n)}$ (g/cm^3)	$e^{(n)}$	$d^{*(n)}$	$g^{(n)}$
A-shale	2745	1508	2.340	0.103	- 0.073	0.345
O-shale	4231	2539	2.370	0.200	0.000	0.145

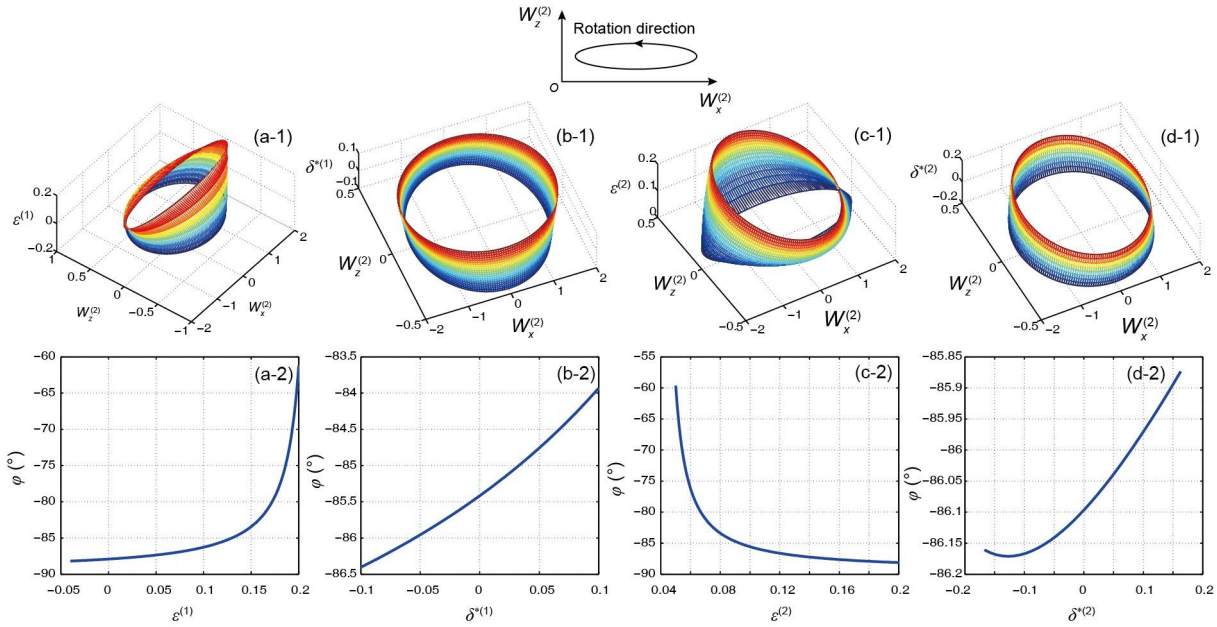

Figure 4 (Color online) Effect of anisotropic parameters on the elliptical-polarization states for interface between A-shale and T-sandstone, where $\theta^{(0)} = 55.05^\circ > \theta_c^{(2)}$ (Model 1). (a-1,2) varying $\varepsilon^{(1)} \in (-0.04, 0.2)$; (b-1,2) varying $\delta^{*(1)} \in (-0.1, 0.1)$; (c-1,2) varying $\varepsilon^{(2)} \in (0.05, 0.2)$; (d-1,2) varying $\delta^{*(2)} \in (-0.167, 0.167)$.

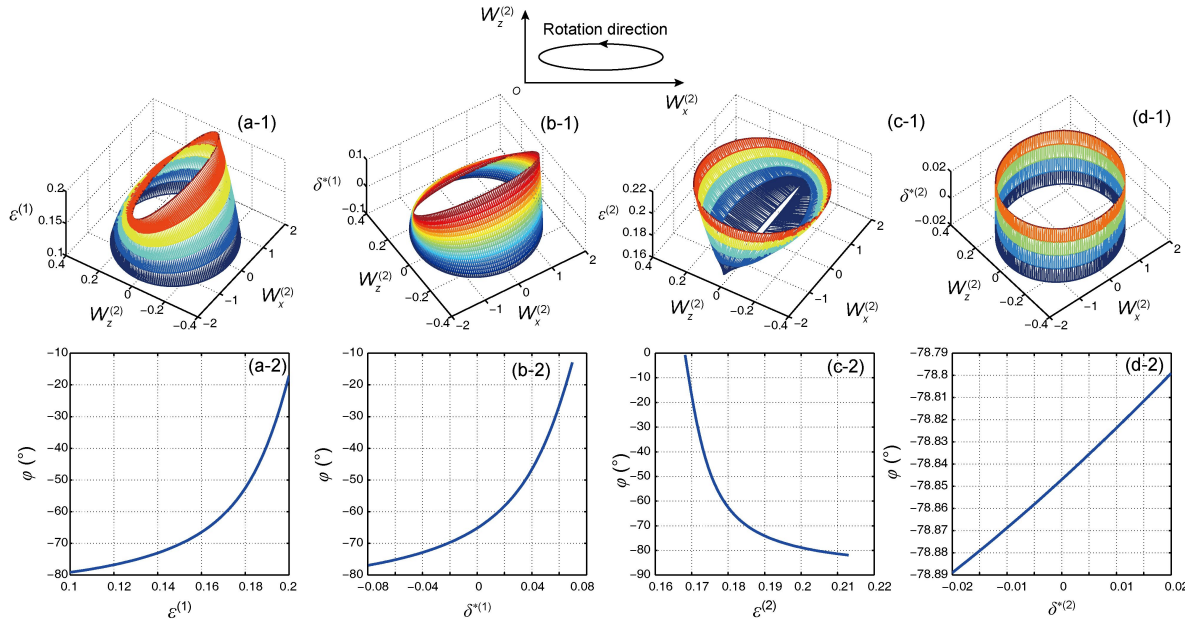

Figure 5 (Color online) Effect of anisotropy parameters on the elliptical-polarization status for interface between A-shale and O-shale, where $\theta^{(0)}=34.58^\circ>\theta_c^{(2)}$, but smaller than $\theta_a^{(2)}$ (Model 1). (a-1,2) varying $\varepsilon^{(1)}\in(0.1,0.2)$; (b-1,2) varying $\delta^{*(1)}\in(-0.08,0.08)$; (c-1,2) varying $\varepsilon^{(2)}\in(0.1682,0.2136)$; (d-1,2) varying $\delta^{*(2)}\in(-0.02,0.02)$.

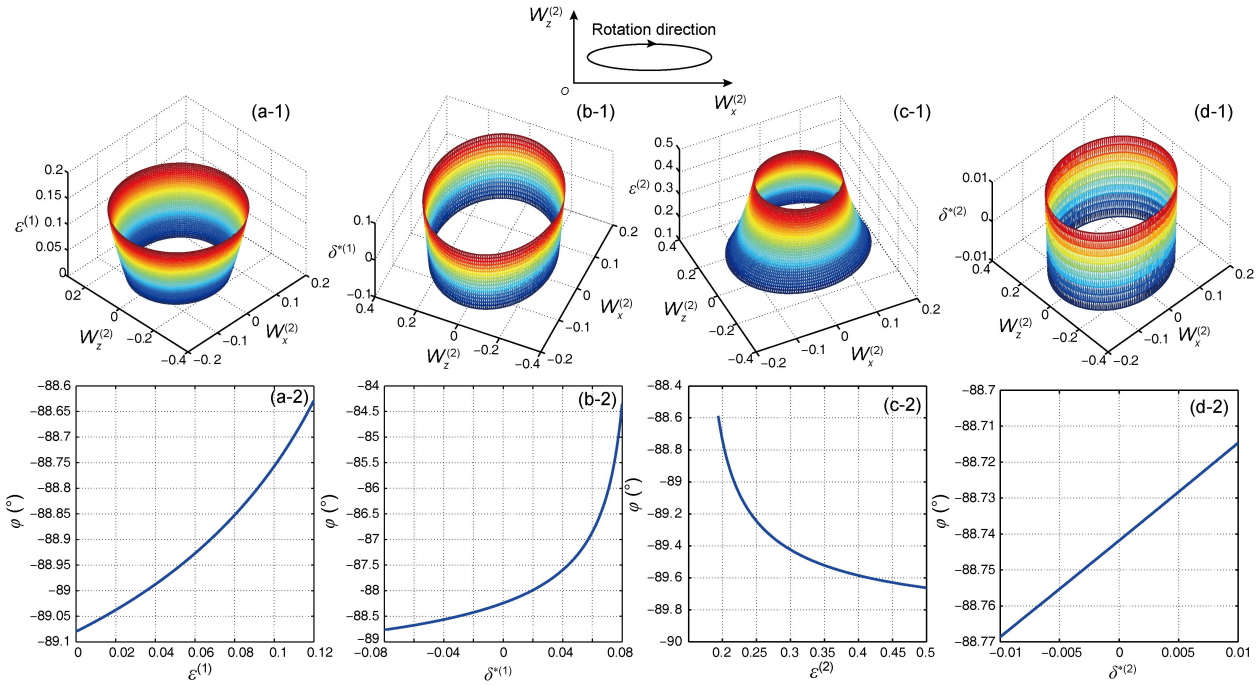

Figure 6 (Color online) Effect of anisotropy parameters on the elliptical-polarization trajectory for interface between A-shale and O-shale, where $\theta^{(2)}=63.91^\circ>\theta_a^{(2)}$(Model 2). (a-1,2) varying $\varepsilon^{(1)}\in(0,0.12)$; (b-1,2) varying $\delta^{*(1)}\in(-0.08,0.08)$; (c-1,2) varying $\varepsilon^{(2)}\in(0.1937,0.5)$; (d-1,2) varying $\delta^{*(2)}\in(-0.01,0.01)$.

elliptical-polarization are greater than the effects of $\delta^{*(1)}$ and $\delta^{*(2)}$ on those of the elliptical-polarization. The inhomgenously refracted P-wave is a right-rotation elliptical-polarization wave (see Figure 4).

For the interface between A-shale and O-shale, the effects of $\varepsilon^{(1)}$, $\delta^{*(1)}$, $\varepsilon^{(2)}$ and $\delta^{*(2)}$ on the size, shape and initial phase angle of the elliptical-polarization at $\theta^{(0)}=34.58^\circ<\theta_a^{(2)}$ (Model 1) are much greater than the effects of these anisotropy parameters on those of the elliptical-polarization at $\theta^{(0)}=63.91^\circ>\theta_a^{(2)}$ (Model 2), as shown in Figures 5 and 6. At the incident-angle $\theta^{(0)}=34.58^\circ$, the inhomogenously refracted P-wave is a right-rotation ellipti-

cal-polarization wave. At the incident-angle $\theta^{(0)} = 63.91^\circ$ it is a left-rotation elliptical-polarization wave.

4 Concluding remarks

We have derived, for the inhomogenously refracted P-wave, the equations of the elliptical-polarization trajectory based on the interface between two VTI media. We have also performed calculations of the polarization states with respect to several varying medium parameters. The results of the calculation were presented in a Poincaré-sphere-like surface. It is interesting to note that its size, shape and initial phase angle of an elliptical-polarization trajectory are not only dependent on the incident-angle, but also very much on the anisotropy the media. For the case where there is no anomalous incident-angle $\theta_a^{(2)}$, the initial phase angle φ of the elliptical-polarization approaches $-90°$ when $\theta^{(0)}$ goes to 90°. For the case where anomalous incident-angle does exist, j approaches to - 90° when $\theta^{(0)}$ goes to $\theta_a^{(2)}$. Meanwhile, in the incident-angle region $\theta^{(0)} \in (\theta_a^{(2)}, 90^\circ)$, the initial phase angle j is very small.

The anomalous incident-angle $\theta_a^{(2)}$ can cause the elliptical-polarization rotation direction of the inhomogenously refracted P-wave to change. Figures 5 and 6 also show that, for the inhomogenously refracted P-wave with an existing anomalous incident-angle $\theta_a^{(2)}$, the influence of the rock anisotropic parameters on the elliptical-polarization state is smaller in the region $\theta^{(0)} \in (\theta_a^{(2)}, 90^\circ)$ than that of $\theta^{(0)} \in (\theta_c^{(2)}, \theta_a^{(2)})$.

Finally, we should note that while the results of derivation and calculations presented in this paper are significant theoretically, it will be more significant if it can be confirmed experimentally and applied to geophysics and to seismic exploration.

This work was supported by Xi'an University of Posts and Telecommunications, and the Physical Sciences Division at The University of Chicago.

1 W. Y. Luo, and R. H. Zhang, Sci. China-Phys. Mech. Astron. **58**(9), 594301 (2015).
2 X. W. Yang, and Y. M. Li, Sci. China-Phys. Mech. Astron. **58**(3), 034601 (2015).
3 J. W. Wang, B. G. Yuan, Y. Cheng, and X. J. Liu, Sci. China-Phys. Mech. Astron. **58**(2), 024302 (2015).
4 C. X. Bi, W. Q. Jing, Y. B. Zhang, and L. Xu, Sci. China-Phys. Mech. Astron. **58**(2), 024301 (2015).
5 Z. L. Li, L. He, R. H. Zhang, F. H. Li, Y. X. Yu, and P. Lin, Sci. China-Phys. Mech. Astron. **58**(1), 014301 (2015).
6 J. X. Qin, R. H. Zhang, W. Y. Luo, Z. H. Peng, J. J. Liu, and D. J. Wang, Sci. China-Phys. Mech. Astron. **57**(6), 1031 (2014).
7 X. X. Cao, T. Li, X. H. Li, C. M. Meng, X. M. Zhou, and W. J. Zhu, Chin. Sci. Bull. **59**(36), 5302 (2014).
8 S. Zhang, and Y. Zhang, Chin. Sci. Bull. **59**(26), 3239 (2014).
9 L. J. Guo, C. J. Min, S. B. Wei, and X. C. Yuan, Chin. Opt. Lett. **11**(5), 0526011 (2013).
10 D. H. Dai, X. S. Wang, S. P. Xiao, and Y. Z. Li, Sci. China Ser. G-Phys. Mech. Astron. **51**(9), 1287 (2008).
11 W. J. Yao, and B. Y. Cao, Chin. Sci. Bull. **59**(27), 3495 (2014).
12 W. Run, P. Z. Tang, A. F. Fang, P. Cai, C. Ye, Y. T. Li, W. H. Duan, N. L. Wang, and Y. Y. Wang, Sci. Bull. **60**(8), 798 (2015).
13 B. Yuan, Z. Z. He, W. Q. Fang, X. Bao, and J. Liu, Sci. Bull. **60**(6), 648 (2015).
14 S. Crampin, R. A. Stephen, and R. McGonigle, Geophys. J. R. Soc. **68**, 477 (1982).
15 B. Hosten, J. Acoust. Soc. Am. **89**, 2745 (1991).
16 P. Lanceleur, H. Ribeiro, and J. D. Belleval, J. Acoust. Soc. Am. **93**, 1882 (1993).
17 K. Helbig, and M. Schoenberg, J. Acoust. Soc. Am. **81**, 1235 (1987).
18 J. M. Carcione, *Wave Fields in Real Media, Wave Propagation in Anisotropic, Anelastic and Porous Media* (Pergamon, An Imprint of Elsevier Science, Amsterdam, Holand, 2001).
19 A. Rüger, *Reflection Coefficients and Azimuthal AVO Analysis in Anisotropic Media* (Society of Exploration Geophysics, Tulsa, USA, 2002).
20 L. Fa, J. P. Castagna, and H. Dong, Sci. China Ser. G-Phys. Mech. Astron. **51**, 823 (2008).
21 L. Fa, M. S. Zhao, Y. C. Liu, L. Wang, Y. Q. Wang, and J. G. Sun, Sci. China Ser. G-Phys. Mech. Astron. **57**, 251 (2014).
22 L. Fa, R. L. Brown, and J. P. Castagna, J. Acoust. Soc. Am. **120**, 3479 (2006).
23 L. Fa, Y. Fa, Y. D. Zhang, P. F. Ding, J. M. Gong, G. H. Li, L. J. Li, S. J. Tang, and M. S. Zhao, Sci. Rep. **5**, 12700 (2015).
24 L. Fa, J. P. Castagna, Z. W. Zeng, R. L. Brown, and M. Zhao, Chin. Sci. Bull. **55**, 2243 (2010).
25 B. A. Auld, *Acoustic Fields and Waves in Solids* (Wiley Vol. 1, New York, USA, 1972).
26 L. Thomsen, Geophysics **51**, 1954 (1986).
27 L. Vernik, and A. Nur, Geophysics **57**, 727 (1992).
28 Z. Wang, Geophysics **67**, 1423 (2002).